Supporting Information

Phosphorous Nitride Dots induced Efficient Advanced Oxidation with Intrinsic Chemiluminescence for Organic Pollutant Degradation

Jing Gou, [a] Tong Sun, [b] Yuxian Zhou, [a] Houjing Liu [a] *

[a.] *College of Chemistry & Chemical Engineering, Guizhou University, Guiyang 550025, China.*
[b.] *College of Chemistry and Environmental Engineering, Sichuan University of Science and Engineering, Zigong, 643000, China.*

**Corresponding Author. Email: hjliu3@gzu.edu.cn*

Chemicals and Reagents. All chemical reagents were used at least of analytical grade and without further purification treatment. Phosphonitrilic chloride trimer (PCT), sodium ascorbate (AA) (99%), p-benzoquinone (BQ), amaranth (AR), Methylene Blue trihydrate (MBT), Methyl Orange (MO), Leucocrystal Violet (LV), Basic Red 5 (BR5), Acid Blue 93 (AB93), Direct Red 28 (DR28), Rhodamine B (RB) and Acid golden yellow G (AYG) were purchased from Shanghai Titan Scientific Co. Ltd (Shanghai, China). Thiourea, sodium oxalate ($Na_2C_2O_4$), L-Histidine (L-His), sodium thiosulphate (Na_2SO_3) was obtained from National Group Chemical Reagent Co. Ltd (Shanghai, China). Dimethyl sulfoxide (DMSO) and hydrogen peroxide (H_2O_2) were bought from Chongqing Chuandong Chemical (Group) Co. Ltd (Chongqing, China). Ethanol was bought from Tianjin Fuyu Fine Chemical Co. Ltd (Tianjin, China). All solution was prepared using deionized water (18.2 MΩ/cm), which was treated with a Mili-Q ultrapure (Chengdu, China) system.

Experimental apparatus. All CL signals were collected using ultra weak chemiluminescence instrument (BPCL-2-TGG, Guangzhou Micro Light Technology Co., Ltd, China). Fluorescence (FL) spectra were obtained on a carry eclipse fluorescence spectrophotometer with excitation wavelength of 290-340 nm, 600 V of high voltage, scan speed 600 nm min−1, and 10 nm excitation slit and 10 nm emission slit. (Varian, Inc., Palo Alto, USA). Transmission electron microscopy (TEM) images of the PNDs were taken by Tecnai G2 F20 S-Twin (FEI, USA), setting the accelerating voltage as 200 kV. The X-ray photoelectron spectra (XPS) were recorded with Thermo Scientific K-Alpha (USA). The X-ray diffraction (XRD) patterns over the range of 10° to 80° were collected by the Powder X-ray diffractometer with Cu Kα radiation (Rigaku Ultma IV, Japan). Electron paramagnetic resonance (EPR) spectra was measured on Bruker E-500, Conditions: microwave power 2.0 mW, modulation frequency 100 kHz, and modulation amplitude 0.1 mT. The cyclic voltammetry curve (scan rate: 0.28 V s-1) in the potential from -0.9 to 0.5 V and electrochemical impedance spectroscopy in the

frequency range of 0.1 ~ 100 KHz for PNDs was recorded with the use of CHI660E (Shanghai chenhua, China) electrochemical workstation. The experiments were carried out in a solution containing 0.05 M H_2SO_4/ 0.1MK_2SO_4=4/1, with bare GCE or modified GCE as the working electrode, saturated glycerol electrode as the reference electrode and platinum wire as the counter electrode. Shimadzu UV-2700 ultraviolet-visible (UV-vis) spectrophotometer (Shimadzu, Japan) was used out to obtain UV-vis absorption spectra. Fourier transform infrared spectroscopy (FT-IR) spectra were obtained with VERTEX70 infrared spectrometer (Brooks, Germany). Degradation intermediates of AR were investigated by quadrupole time-of-flight liquid chromatography-mass spectrometer (Agilent Technology Co., Ltd, China).

Preparation of PNDs. The PNDs were fabricated using a solvothermal method with phosphonitrilic chloride trimer (PCT). In a typical process, 20 mg PCT was mixed with 20mL ethanol and transferred to a poly(tetrafluoroethylene) (Teflon)-lined autoclave (100 mL). Then, the mixture was heated at 180 °C for 12 h. After the completion of the hydrothermal reaction, this autoclave was allowed to cool down at room temperature and this solution was then dialyzed through a dialysate bag (3500 Da) against deionized water at 25°C for 24 h. Water used in this process changed after every 6 h. The PNDs were included in ethanol transparent liquid. To obtain PNDs solid, ethanol was removed via rotary evaporation method at 50 °C. Finally, the acquired products were dried and kept in a vacuum for further use. And when being used, the resulting product was dissolved into deionized water to form a solution containing PNDs (1mg/mL) for later experiments.

Chemiluminescence analysis. All CL signals were obtained using the static injection CL analysis. To ensure the accuracy and reliability of the experimental data, all CL experiments were performed three times in parallel toward every sample. Typically, for PNDs-SO_3^{2-} and PNDs-H_2O_2-SO_3^{2-} CL systems, 400μL PNDs, 200μL H_2O_2 solution, and 400μL PBS solution were mixed and placed in the quartz vial (2 mL). Then 200 μL SO_3^{2-} was quickly injected to trigger the reaction, followed by the collection of CL signal. For H_2O_2-PNDs and H_2O_2-SO_3^{2-} systems, 400 μL PBS solution containing 200 μL H_2O_2 solution was placed in the quartz vial. When 200 μL of PNDs or SO_3^{2-} solution was automatically injected, the reaction was rapidly initiated and the CL signal was detected by the PMT and exported to the computer for data acquisition. The negative voltage of the photomultiplier tube (PMT) was set at 0.8 kV; the time interval was set as 0.1 s. The CL spectrum of all systems was obtained by the BPCL luminescence analyzer with optical filters (350-640 nm), which were placed between the quartz vial and the detector.

Degradation of the amaranth. Using amaranth (AR) as a pollutant model, the potential application of PNDs-H_2O_2-SO_3^{2-} system in water treatment was discussed. Firstly, 2 mL of PNDs (1mg/mL) and 0.01 mL AR (10^{-2} mol/L) were mixed with 14 mL PBS (PH 3.0) solution. Then, 2 mL H_2O_2 solution (0.1 mol/L) was added to the above mixture. Finally, 2 mL SO_3^{2-} (5×10^{-2} mol/L) solution was injected to initiate the degradation. subsequently, the obtained solution was constantly stirred. At an interval of time, the reaction solution was taken out and used for AR concentration determination using a UV–vis

spectrophotometer at 520 nm. The AR removal rate was calculated by the following formula: removal rate (%) = (C_0-Ct)/C_0*100%.

Characterization of PNDs. The morphologies of the PNDs were characterized using transmission electron microscopy (TEM) and high-resolution TEM (HRTEM). The TEM image reveals a uniform distribution of PNDs with sizes ranging from 0.5 nm to 4.5 nm, predominantly centered at approximately 1.5 nm (Fig. S1a). The HRTEM image confirms the highly crystalline nature of the PNDs, with lattice fringes corresponding to the (200) crystal plane at a spacing of approximately 0.19 nm (Fig. 1a). The crystal structure of the PNDs was further examined using powder X-ray diffraction (XRD). The XRD pattern in Fig. 1b displays distinct diffraction peaks at 22.9°, 32.6°, 46.8°, and 58.24°, corresponding to the (100), (110), (200), and (211) crystal faces, respectively. Notably, the characteristic diffraction peaks of the precursor (PCT) were no longer observed, indicating the successful formation of PNDs through the solvothermal reaction. X-ray photoelectron spectroscopy (XPS) was conducted to investigate the chemical composition and states of the synthesized PNDs. The XPS survey scan spectrum in Fig. S1b shows characteristic peaks corresponding to P2p, N1s, and O1s. The P2p XPS spectrum exhibits two prominent peaks at 133.19 eV and 134.09 eV, which can be attributed to the $2p_{3/2}$ and $2p_{1/2}$ states, respectively (Fig. 1c). These peaks likely arise from the overlapping spectrum of N-P=N and P=O bonds. The O1s spectrum further confirms the presence of P=O and P-O bonds, with two strong peaks observed at 530.7 eV and 532.40 eV. In the N1s high-resolution spectrum, two peaks are observed at 400.76 eV and 399.28 eV, corresponding to sp2 hybridized N atoms (P-N=P) and N-H bonds, respectively[1]. These results indicate the formation of PNDs with a π-conjugated electronic structure composed of P and N elements. Additionally, Fourier transform infrared spectra (FT-IR) measurements was performed to investigate the surface functionalization of the synthesized nanomaterials. The FT-IR spectrum in Fig. S1c reveals several new peaks in the ranges of 973 ~ 1400 cm-1, 743 cm-1, and ~500 cm-1, attributed to the P=N stretching vibration, P-N stretching vibration, and unreacted P-Cl bonds, respectively[2], confirming the characteristic chemical structures of the PNDs. Moreover, two absorption bands centered at ~3000 cm-1 and ~1700 cm-1 correspond to the stretching and bending vibrations of the N-H bond, suggesting the presence of -NH_2^+ functional groups on the surface of the PNDs[3]. Clear peaks at ~1600 cm-1 and ~800 cm-1 indicate the presence of P=O and P-O groups, respectively, indicating the formation of oxygen-containing groups on the surface of the PNDs. Additionally, a reduction peak (Ep = -0.655 V) observed in the cyclic voltammetry curve (CV) of the PNDs (Fig. S1d) suggests the presence of reducing amino groups on the material surface. The electrochemical impedance spectrum (EIS) of PNDs (Fig. S1e) showed smaller semicircles in the high-frequency region than that of PCT, indicating lower electron-transfer resistance and higher interfacial charge-transfer activity of PNDs. Furthermore, Mott-Schottky plots (at 600 Hz) further confirmed the electron transfer kinetics of the PNDs (Fig. S1f). PNDs have the properties of N-type semiconductors (the curves have positive

slopes) with higher carrier densities. Notably, the presence of oxygen-containing and -NH_2^+ groups facilitated the formation of hydrogen bonds with organic pollutants and PNDs displayed efficient electron transfer rates, thereby exhibiting significant potential for adsorptive degradation and catalytic applications towards these contaminants. The optical property of the PNDs were explored through UV–vis absorption spectra and fluorescence (FL) spectra. The UV–vis absorption spectrum exhibits a maximum emission wavelength at 265 nm (Fig. S2a), indicating good aqueous dispersion. The FL spectrum of the PNDs displays a strong emission centered at 396 nm with an excitation wavelength of 310 nm. Furthermore, the FL property of the PNDs shows dependence on the excitation wavelength (Fig. S2b), possibly attributed to the size and quantum effects in nanomaterials. Considering the excellent luminescent properties of the PNDs, we envision their potential as an ideal CL emitter with efficient electron transfer.

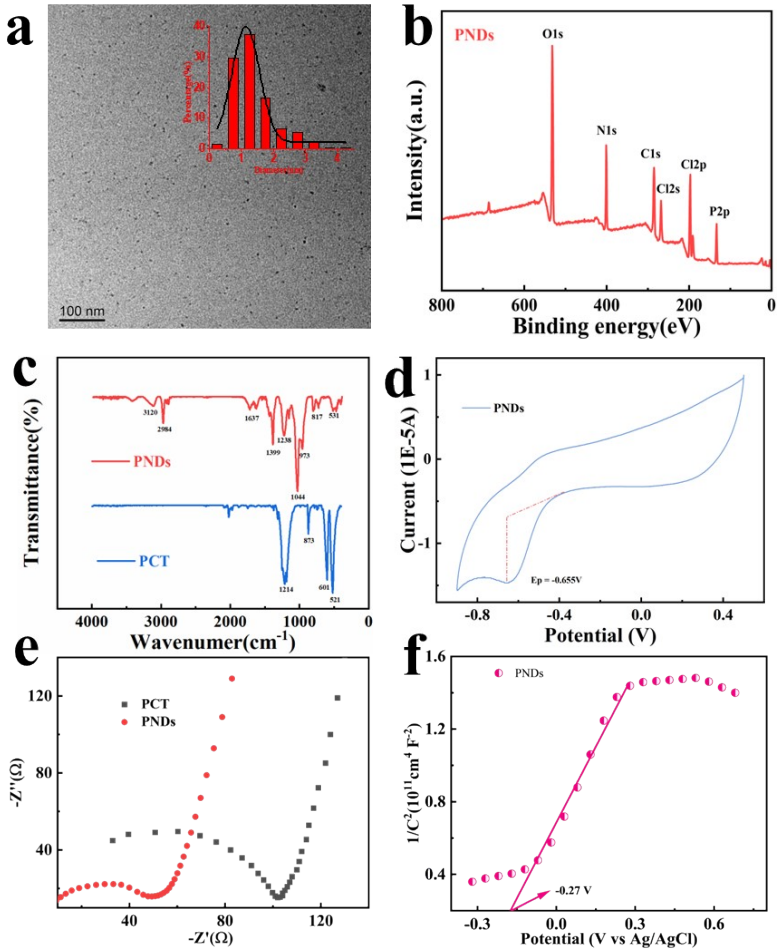

Fig. S1. (a) TEM images of PNDs. (b) The XPS spectra of PNDs. (c) FT-IR spectra of the synthesized PNDs. (d) The cyclic voltammetry curve (CV) of PNDs. (e) The electrochemical impedance spectrum (EIS) of PNDs. (f) The Mott-Schottky plots of PNDs.

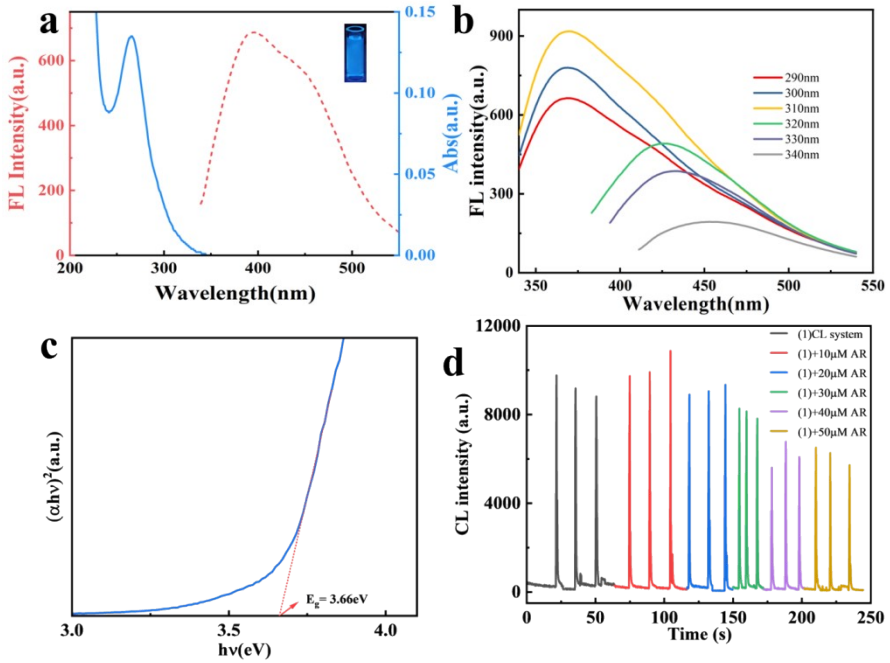

Fig. S2. (a)The UV-Vis absorption and the FL. (b) FL spectra of PNDs at different excitation wavelengths. (c) Band gap value of PNDs. (d) The influence of contaminant AR on CL.

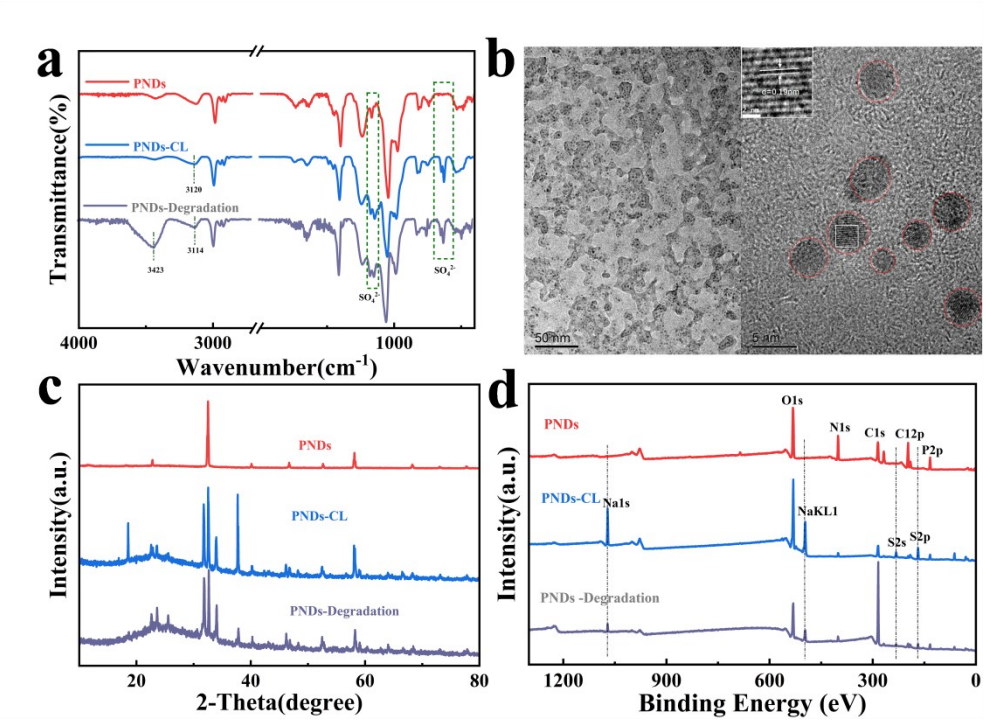

Fig. S3. (a) FT-IR, (c) XRD and (d) XPS spectra of PNDs after CL reaction and degradation reaction. (b) TEM and HRTEM images of PNDs after CL reaction. (PNDs-CL and PNDs-Degradation denote the PNDs after reaction with H_2O_2-SO_3^{2-} and H_2O_2-SO_3^{2-}-AR systems, respectively).

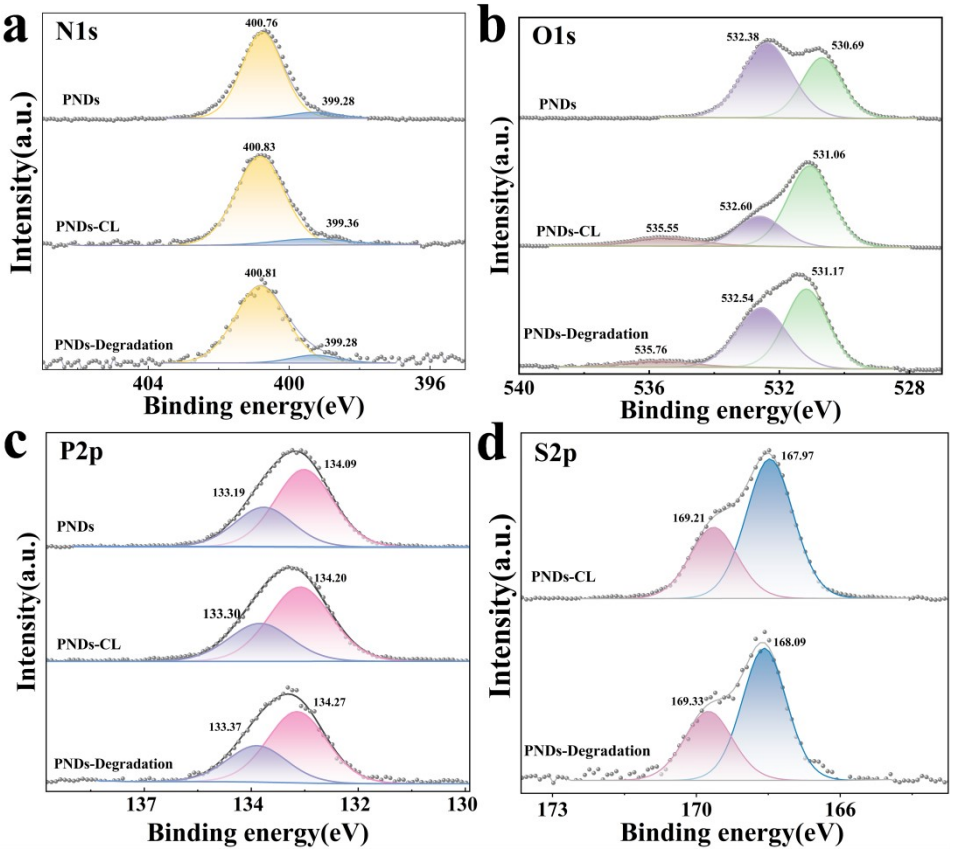

Fig. S4. The XPS spectrum in (a) the N1s, (b) O1s (c) P2p and (d) S2p region of PNDs, PNDs after CL reaction and PNDs after degradation reaction.

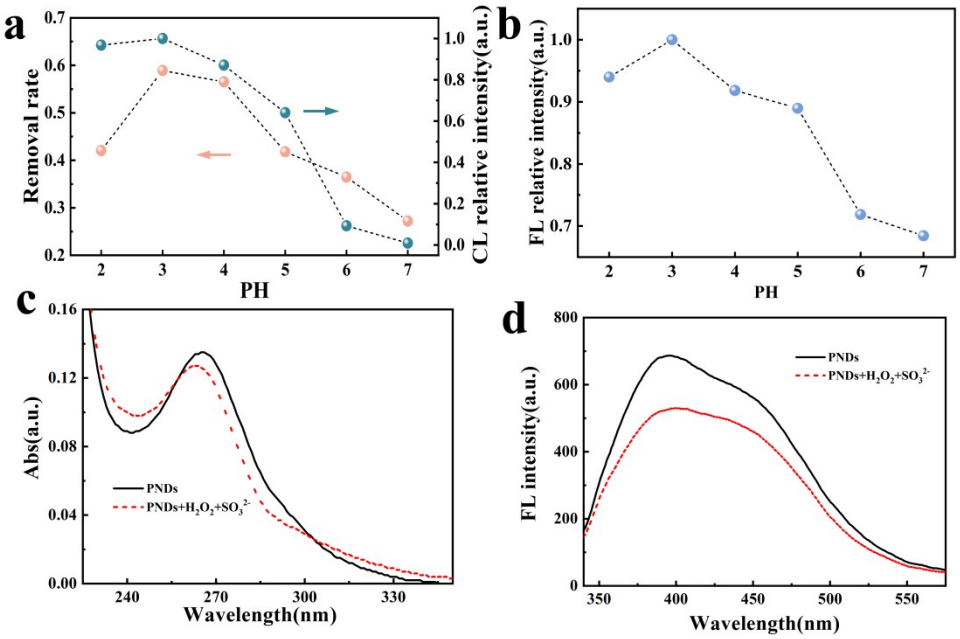

Fig. S5. (a) The relationship between CL and AR removal rate in PNDs-H_2O_2-SO_3^{2-} system under different PH. (b) The FL of PNDs at different PH. (c) UV−vis absorption and (d) FL spectra of PNDs before and after CL reaction.

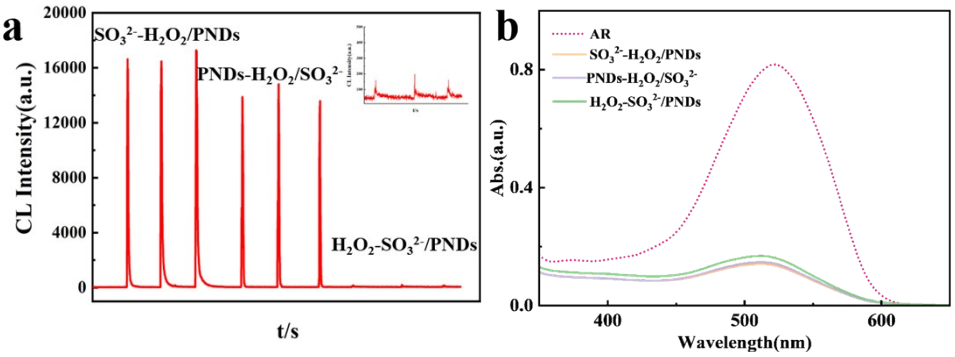

Fig. S6. (a) CL intensity and (b) degradation efficiency for different injection order.

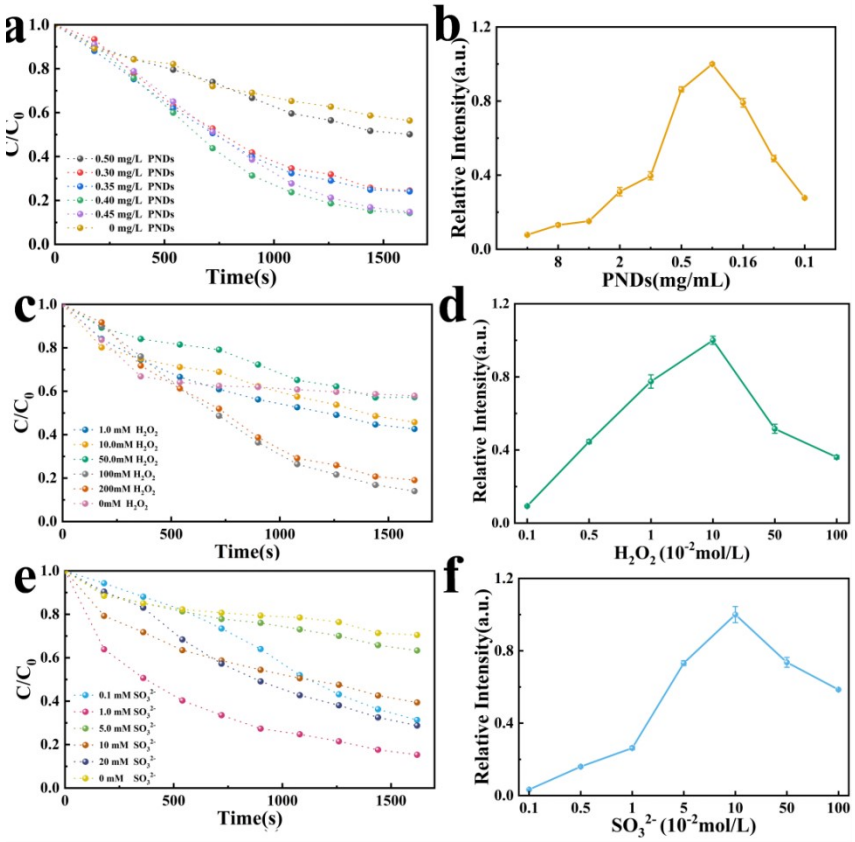

Fig. S7. Degradation curves of AR by different concentrations of (a) PNDs, (c) H_2O_2 (PH 3.0, 0.4mg/mL PNDs, 0.1mol/L SO_3^{2-}), (e) SO_3^{2-} (PH 3.0, 0.4mg/mL PNDs, 0.1 mol/L H_2O_2). Effect of different (b) PNDs, (d) H_2O_2, (f) SO_3^{2-} concentration on CL.

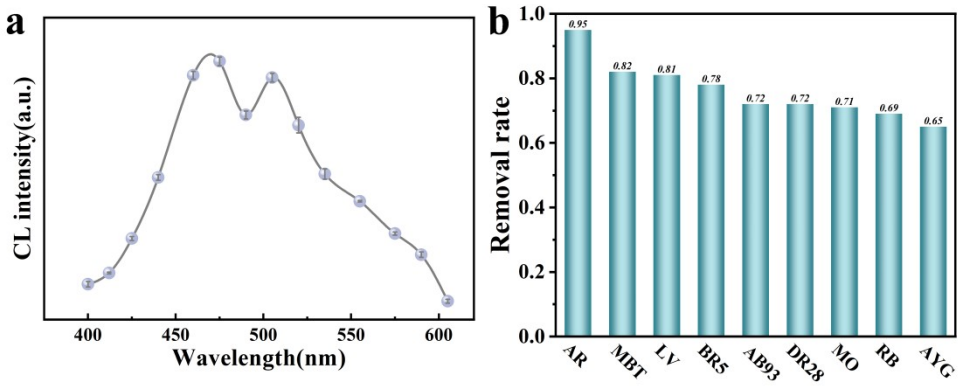

Fig.S8. (a) The CL spectra of PNDs-H_2O_2-SO_3^{2-} system. (b) Removal rate of similar pollutants in PNDs-H_2O_2-SO_3^{2-} system.

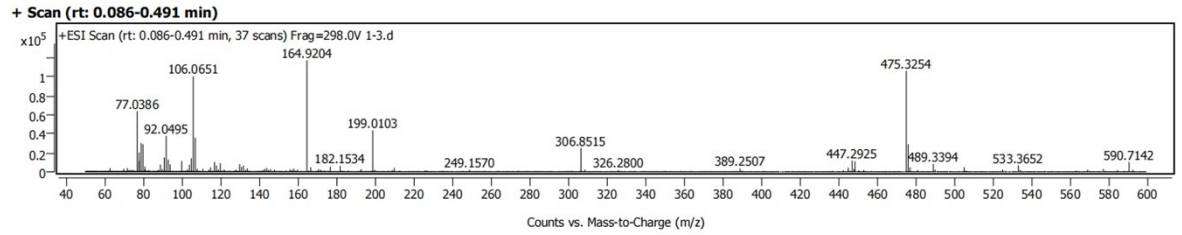

Fig.S9. HPLC-MS spectra of AR after degradation in PNDs-H_2O_2-SO_3^{2-} system.

Table S1. Application of AOPs in the treatment of industrial textile dye wastewater.

Process	Target pollutants	Experimental conditions	Degradation rate	References
AOPs (PCN/Co_3O_4-HClO)	Methylene blue(MB)	pH:3.0 $[HClO]_0$:200 μM MB_0:20 mg/L $[catalyst]_0$:0.5 g/L Reaction time:30min	98.2%	[4]
Photocatalytic (Mn–TiO2)	Malachite green (MG)	MB_0:0.4 mg/L $[catalyst]_0$:0.4M Reaction time:105min	96%	[5]
Photoelectrocatalysis (UIO-66@TNF/Ti-foam)	Rhodamine B (RhB)	pH:7.0 RhB_0:5 mg/L bias potential: 2.0 V Reaction time: 200min	99.1%	[6]
SR-AOPs (Fe_3O_4/Graphene Oxide/ PS)	RhB	RhB：20 ppm $K_2S_2O_8$：1.5 mM pH：4.34 Solution pH：4.7 Reaction time：50 min	95%	[7]
SR-AOPs (Hydroxylamine (HA)/Fe(II)/PS/ Cu (II))	Acid Orange 7 (AO7)	PH:3 $[AO7]_0$: 25 Mm $[Fe(II)]_0$: 10 mM $[Cu(II)]_0$: 0-5 mM $[HA]_0$: 0.15 mM $[PS]_0$: 0.7 mM	94.7%	[8]
Photo-Fenton process ($Cu_2Cl(OH)_3$ nanoflowers)	RhB	Catalyst: 0.1 g H_2O_2: 2 μL (30 wt%) RhB: 200 mL (10 $mg \cdot L^{-1}$) Reaction time:30 min	98.5%	[9]
This work (AOPs, PNDs-H_2O_2-SO_3^{2-})	AR	PH:3 $[Catalyst]_0$: 0.4mg/mL $[H_2O_2]_0$: 100mM $[SO_3^{2-}]_0$: 1mM [AR]: 18 $mg \cdot L^{-1}$ Reaction time:30 min	nearly 100%	/

References

1. P. Gao, Z. Huang, J. Tan, G. Lv and L. Zhou, *ACS Sustain. Chem. Eng.*, 2022, **10**, 4634-4641.
2. M. Zhang, Y. Li, C. Bai, X. Guo, J. Han, S. Hu, H. Jiang, W. Tan, S. Li and L. Ma, *ACS Appl. Mater. Interfaces*, 2018, **10**, 28936-28947.
3. X. Wu, J. Shu, B. Feng, L. Yang, J. Lan, F. Li, P. Xi and F. Wang, *Chem. Commun.*, 2019, **55**, 4719-4722.
4. Q. Guo, H. Song, M. Sun, X. Yuan, Y. Su and Y. Lv, *Journal of Hazardous Materials*, 2022, **429**.
5. S. P. Keerthana, R. Yuvakkumar, G. Ravi, A. G. Al-Sehemi and D. Velauthapillai, *Chemosphere*, 2022, **306**.
6. X. Zhang, X. Liang, M. Xu, J. Wang, F. Wang and M. Chen, *Chemosphere*, 2023, **312**.
7. X. Yang, Q. Zhang, W. Gu, F. Teng, *J. Cryst. Growth*, 2020, **541**.
8. M.N. Pervez, W. He, T. Zarra, V. Naddeo, Y. Zhao, *Water* ,**12**.
9. X. Liu, B. Yuan, J. Zou, L. Wu, L. Dai, H. Ma, K. Li, J. Ma, *Chemosphere,*2020 ,**238**.